Free Radical Biology & Medicine 50 (2011) 1760–1770

Contents lists available at ScienceDirect

Free Radical Biology & Medicine

journal homepage: www.elsevier.com/locate/freeradbiomed

Original Contribution

1,4-Diamino-2-butanone, a wide-spectrum microbicide, yields reactive species by metal-catalyzed oxidation

Chrislaine O. Soares [a], Maria Julia M. Alves [a], Etelvino J.H. Bechara [a,b,*]

[a] Departamento de Bioquímica, Instituto de Química, Universidade de São Paulo, 05508–900 São Paulo, SP, Brazil
[b] Departamento de Ciências Exatas e da Terra, Instituto de Ciências Ambientais, Químicas e Farmacêuticas, Universidade Federal de São Paulo, Diadema, SP, Brazil

ARTICLE INFO

Article history:
Received 6 September 2010
Revised 22 March 2011
Accepted 28 March 2011
Available online 3 April 2011

Keywords:
1,4-Diamino-2-butanone
α-Aminoketones
α-Oxoaldehydes
Reactive oxygen species
Ferritin
Transferrin
Oxidative damage
Free radicals

ABSTRACT

The α-aminoketone 1,4-diamino-2-butanone (DAB), a putrescine analogue, is highly toxic to various microorganisms, including *Trypanosoma cruzi*. However, little is known about the molecular mechanisms underlying DAB's cytotoxic properties. We report here that DAB (pK_a 7.5 and 9.5) undergoes aerobic oxidation in phosphate buffer, pH 7.4, at 37 °C, catalyzed by Fe(II) and Cu(II) ions yielding NH_4^+ ion, H_2O_2, and 4-amino-2-oxobutanal (oxoDAB). OxoDAB, like methylglyoxal and other α-oxoaldehydes, is expected to cause protein aggregation and nucleobase lesions. Propagation of DAB oxidation by superoxide radical was confirmed by the inhibitory effect of added SOD (50 U ml^{-1}) and stimulatory effect of xanthine/xanthine oxidase, a source of superoxide radical. EPR spin trapping studies with 5,5-dimethyl-1-pyrroline-1-oxide (DMPO) revealed an adduct attributable to DMPO–$HO^•$, and those with α-(4-pyridyl-1-oxide)-*N*-*tert*-butylnitrone or 3,5-dibromo-4-nitrosobenzenesulfonic acid, a six-line adduct assignable to a $DAB^•$ resonant enoyl radical adduct. Added horse spleen ferritin (HoSF) and bovine apo-transferrin underwent oxidative changes in tryptophan residues in the presence of 1.0–10 mM DAB. Iron release from HoSF was observed as well. Assays performed with fluorescein-encapsulated liposomes of cardiolipin and phosphatidylcholine (20:80) incubated with DAB resulted in extensive lipid peroxidation and consequent vesicle permeabilization. DAB (0–10 mM) administration to cultured LLC-MK2 epithelial cells caused a decline in cell viability, which was inhibited by preaddition of either catalase (4.5 μM) or aminoguanidine (25 mM). Our findings support the hypothesis that DAB toxicity to several pathogenic microorganisms previously described may involve not only reported inhibition of polyamine metabolism but also DAB pro-oxidant activity.

© 2011 Elsevier Inc. Open access under the Elsevier OA license.

Similar to 5-aminolevulinic acid (ALA), a heme precursor implicated in acquired and inborn porphyria [1,2], and aminoacetone (AA), a threonine and glycine catabolite suggested to be related to diabetes manifestations [3,4], the microbicide 1,4-diamino-2-butanone (DAB) bears an amino group vicinal to a carbonyl group (Scheme 1), rendering DAB prone to fast enolization and subsequent metal-catalyzed oxidation by dissolved dioxygen. Reactive oxygen species, ammonium ions, and α-oxoaldehydes are the main products of ALA and AA chemical oxidation [5–7]. α-Oxoaldehydes such as 3,4-dioxovaleric acid and methylglyoxal, produced by ALA and AA, respectively, have been shown to be highly cytotoxic and genotoxic electrophiles [6,8]. They partake in electrophilic attack on amino groups of proteins and nucleobases yielding Schiff bases, Maillard adducts, and ethane DNA adducts, which are putative biomarkers of oxidative and carbonyl stress in aging-related diseases and diabetes [9,10]. Protein aggregation and dysfunction due to cross-linking with these reactive dicarbonyls may underlie the clinical manifestations of such disorders.

Recently DAB has been reported to be toxic to several pathogens, including *Trypanosoma cruzi*, the etiologic agent of Chagas disease [11]. Other pathogenic microorganisms reported to be affected by DAB include *Leishmania amazonensis*[12], *Giardia lamblia*[13], and *Tritrichomonas foetus*[14]. It is thought that the major effect of DAB upon microorganisms is the inhibition of ornithine decarboxylase (ODC; $K_i = 0.9$ μM), the enzyme that catalyzes the first step in polyamine biosynthesis culminating in cell arrest [15,16]. Polyamines have long been known to play fundamental roles in growth, development, cellular differentiation, macromolecular stabilization, and apoptosis [17,18].

Here, we report that DAB undergoes metal-catalyzed aerobic oxidation in phosphate buffer to yield an α-oxoaldehyde and reactive oxygen species (ROS), which could drive oxidative damage to added ferritin, apo-transferrin, and biomimetic liposomes. Superoxide radical is shown to propagate the oxidation of DAB to 1-imino-4-amino- 2-butanone, whose hydrolysis yields 4-amino-2-oxobutanal (oxoDAB) and NH_4^+ ion. As expected from Schiff-type additions, further formation of a pyrrole adduct of oxoDAB with remaining DAB is demonstrated. Finally, DAB is shown to promote oxoDAB- and ROS-mediated loss of epithelial cell viability, revealing a mechanism that may contribute to the reported DAB toxicity to pathogenic microorganisms.

* Corresponding author. Fax: +55 11 30913869.
E-mail address: ejhbechara@gmail.com (E.J.H. Bechara).

0891-5849 © 2011 Elsevier Inc. Open access under the Elsevier OA license.
doi:10.1016/j.freeradbiomed.2011.03.033

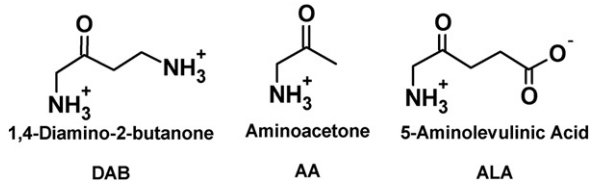

Scheme 1. Chemical structures of 1,4-diamino-2-butanone, aminoacetone, and 5-aminolevulinic acid.

Materials and methods

Materials

DAB, Chelex-100, diethylenetriaminepentaacetic acid (DTPA), desferrioxamine, bovine blood Cu,Zn superoxide dismutase (SOD), horse spleen ferritin (HoSF), bovine apo-transferrin, bovine liver catalase (CAT), ammonia diagnostic kit, $FeSO_4$, $CuSO_4$, xanthine, bovine milk xanthine oxidase, mannitol, semicarbazide, *N*-acetyl-L-cysteine (NAC), 5,5-dimethyl-1-pyrroline-1-oxide (DMPO), α-(4-pyridyl-1-oxide)- *N*-*tert*-butylnitrone (POBN), Triton X-100, phosphatidylcholine, and cardiolipin were purchased from Sigma–Aldrich (St. Louis, MO, USA). Acetic acid, NaOH, $Na_2HPO_4 \cdot 12H_2O$, $NaH_2PO_4 \cdot H_2O$, and NaCl were supplied by Merck (Darmstadt, Germany). The spin trap 3,5-dibromo-4-nitrosobenzenesulfonic acid (DBNBS) was prepared as previously described [19]. All other chemicals were of analytical grade. DAB stock solutions were prepared with degassed 18 MΩ Milli-Q water and kept under nitrogen atmosphere. All buffers were pretreated with Chelex-100.

Oxygen consumption

Oxygen uptake was measured using a Clark-type electrode in a sealed glass chamber (Hansatech Instruments Ltd, Norfolk, UK). All experiments were carried out in air-equilibrated 100 mM phosphate buffer, pH 7.4, at 37 °C.

EPR spin trapping experiments

EPR spectra of DMPO, POBN, and DBNBS spin adducts were recorded in a Brucker EMX spectrometer at room temperature. All spectra were recorded after 20 min of reagent incubation in 100 mM phosphate buffer, pH 7.4, at 25 °C. The instrumental conditions were as follows: microwave power, 20.21 mW; modulation amplitude, 0.15 mT; time constant, 164.84; and gain, 1.12×10^6.

UV–Vis and fluorescence spectral analyses

DAB decay at 37 °C was monitored in the region of 200 to 500 nm in a Varian Cary 50 Bio UV–Vis spectrophotometer (Australia Pty Ltd) and spectrofluorimetrically using SpexFluorolog 1681 equipment (Horiba Scientific, Ann Arbor, MI, USA). Ferritin and apo-transferrin were incubated with 1.0–10 mM DAB in 100 mM phosphate buffer, pH 7.4, at 37 °C. Tryptophan fluorescence data were obtained at 280/345 nm after 2 h incubation using a Spectra Max M2^e microplate reader (Molecular Devices, Sunnyvale, CA, USA).

Product analysis

DAB oxidation products from 3.0 mM DAB in air-equilibrated 100 mM phosphate buffer, pH 7.4, at 37 °C, under agitation for 2 h, were analyzed by HPLC. Products were separated using a Waters HPLC system (Waters Corp., Milford, MA, USA) equipped with a photodiode array detector and a fluorescence detector. The HPLC conditions were adapted from Itakura et al. [20] as follows: isocratic mobile phase methanol:water (10:90, v/v) with 0.2% acetic acid, Supelco column C_{18} (250×4.6 mm, 5 μm particle size), flow rate 0.70 ml min^{-1}. All analyses were performed at room temperature.

Electrospray ionization mass spectra (ESI/MS) were obtained in an LCD Ion Max Advanced spectrometer (Thermo Finnigan, Waltham, MA, USA) in positive mode under the following conditions: voltage, 10 V; nitrogen used as the sheath gas at 20 psi; temperature, 275 °C; spray voltage, 4.5 kV; capillary voltage, 10 V; tube lens offset, 5 V. Fractions collected under the HPLC peaks were concentrated and injected directly into the ESI/MS spectrometer.

Ammonia was assayed spectrophotometrically in the final reaction mixture using a commercial kit (Ammonia Diagnostic Kit; Sigma) based on the NADPH-dependent enzymatic amination of α-oxoglutarate.

Ferritin iron release

Horse spleen ferritin was purified on Sephadex G-25 as described by Oteiza et al. [21] to remove loosely bound iron. Protein concentration was determined by the classic method of Bradford [22]. Iron released by DAB from ferritin was followed by measuring the increase in absorbance at 530 nm due to chelation of Fe(II) by bathophenanthroline sulfonate ($A_{530} = 22.14$ cm^{-1} mM^{-1}). Experimental conditions were 1.0 mM bathophenanthroline sulfonate and 2.5 mg ml^{-1} HoSF in 100 mM phosphate buffer, pH 7.4, at 37 °C, in the presence of 1.0–10 mM DAB with or without 5–400 U ml^{-1} SOD, incubated for 2 h.

Lipid peroxidation

Liposomes made from phosphatidylcholine:cardiolipin (80:20) were prepared by sonication according to Oteiza and Bechara [23]. To evaluate the effects of DAB on lipid peroxidation, 0.60 mM phospholipid was incubated in 100 mM phosphate buffer, pH 7.4, at 37 °C, for 60 min, in the presence of 1.0–5.0 mM DAB and 3 μM Fe(II)EDTA or Cu(II). The reaction was stopped by addition of 4% (final concentration) *tert*-butylated hydroxytoluene. Lipid peroxidation was determined by HPLC using fluorimetric detection of thiobarbituric acid–malondialdehyde (TBA–MDA) adducts against a standard curve obtained with 1,1,3, 3-tetramethoxypropane [24,25], after minor modification as follows. The separation was achieved using a Supelco column C_{18} (250×4.6 mm, 5 μm particle size) and a mobile phase made from KH_2PO_4–KOH (5 mM, pH 7.0) and methanol (50:50 v/v), with a flow rate of 0.7 ml min^{-1}. The TBA–MDA adduct was monitored at $\lambda_{ex} = 515$ nm and $\lambda_{em} = 553$ nm.

5(6)-Carboxyfluorescein (CF) was encapsulated into phosphatidylcholine:cardiolipin liposomes (80:20) prepared by sonication according to Oteiza et al. [23], under self-quenching conditions (0.10 M). CF release from DAB-treated liposomes was measured as the increase in fluorescence at 550 nm (excitation 490 nm) due to dilution of the probe in the external medium. Liposomes (0.60 mM phospholipids) were incubated in 100 mM phosphate buffer, pH 7.4, at 37 °C, for 24 h. Complete release was obtained by addition of Triton X-100 (0.2% final concentration). CF release was calculated as $(F_1/F_0) \times 100$, where F_1 is the fluorescence at 550 nm in the absence of Triton X-100, and F_0 is the fluorescence at 550 nm in the presence of Triton X-100.

Cell culture and treatments

LLC-MK2, a monkey kidney epithelial cell line, was maintained in minimum essential medium (MEM) (Invitrogen, Carlsbad, CA, USA) supplemented with 10% fetal bovine serum (FBS) (Cultilab, Campinas, SP, Brazil) at 37 °C and 5% CO_2. For cell viability assays, LLC-MK2 cells were seeded in a 24-well plate at a density of 5×10^4 cells/well 24 h before the treatments. Cell viability was determined using 3-[4,5-dimethylthiazol-2-yl]-2,5-diphenyl tetrazolium bromide (MTT; Sigma–Aldrich). Viability was determined by the level of reduced MTT measured at 570 nm, expressed as a percentage of the control as a reference.

Statistical analysis

Data represent at least three independent experiments, expressed as means ± SD. The Student *t* test or ANOVA was employed for statistical analysis, using a significance of $p<0.05$.

Results

Oxygen uptake

Addition of DAB (3.0 mM) to normally aerated 100 mM phosphate buffer ([O_2] ~200 μM [26]), pH 7.4, immediately triggers oxygen consumption (Fig. 1, curve a). Maximum oxygen uptake rates (k_{obs}, s^{-1}) respond linearly to the increase in DAB concentration (1.0–5.0 mM) and allow the calculation of an apparent second-order rate constant, k_2, as 0.100 ± 0.007 M^{-1} s^{-1} (Fig. 1, inset). The addition of desferrioxamine or DTPA (1.0 mM) to the system inhibited oxygen consumption by DAB (Fig. 1, curves b and c), suggesting the presence of contaminant metals that are putatively able to catalyze oxidation reactions by dioxygen [27]. Accordingly, medium supplementation with 3.0 or 10 μM Fe(II)EDTA or 3.0 μM aqueous Cu(II) resulted in the acceleration of oxygen consumption by DAB (Fig. 1, curves d, e, and f). Controls consisting of buffer and added transition metals do not show oxygen consumption (Fig. 1, curves g and h). Copper(II)-catalyzed DAB oxidation was threefold faster than with Fe(II)EDTA. Transition metal ions catalyze both the initiation and the propagation steps once they originate hydroxyl radical by Fenton-type reactions, which can initiate further events of DAB hydrogen abstraction and oxygen uptake [28].

Addition of scavengers of reactive oxygen species to the reaction mixture inhibits oxygen uptake (Table 1). With regard to the Fe(II)EDTA (3 μM)-catalyzed DAB (3.0 mM) oxidation, the observed inhibitory effects of Cu,ZnSOD (35%), semicarbazide (43%), CAT (20%), and mannitol (36%) attest to the intermediacy of $O_2^{\bullet-}$, H_2O_2, and $HO^{\bullet}$ species, respectively. Autoxidation of ferrous ion may contribute as a source of $O_2^{\bullet-}$ radical that can initiate DAB oxidation. CAT and GSH decreased the observed rate of Cu(II)-catalyzed oxygen uptake by 50 and 83%, respectively, whereas the other scavengers had no significant effects, suggesting formation of high amounts of H_2O_2 by the Cu(II)-catalyzed reaction. Hydrogen peroxide may originate highly oxidizing hydroxyl radical by a Fenton-type reaction [27], thereby amplifying DAB oxidation by hydrogen abstraction.

Table 1
Effects of ROS scavengers on the rate of oxygen uptake by DAB in the presence of transition metal ions.

System	% Inhibition	
	$Cu(II)_{aq}$	Fe(II)EDTA
Catalase	52 ± 0.94	20 ± 0.96
Mannitol	8.65 ± 1.38	36 ± 8.07
Semicarbazide	No	43 ± 3.26
SOD	2.69 ± 0.49	35 ± 1.58
GSH	83 ± 0.27	9.35 ± 3.01

Oxygen uptake by 3 mM DAB in 100 mM phosphate buffer, pH 7.4, at 37 °C in the presence of 3 μM Cu(II) or Fe(II)EDTA was measured. Catalase, 4.5 μM; mannitol, 50 mM; semicarbazide, 5 mM; SOD, 50 U ml^{-1}; and GSH, 1 mM.

Co-oxidation of DAB and xanthine in the presence of xanthine oxidase, a well-known source of $O_2^{\bullet-}$, confirms (Fig. 2, curve c) the ability of $O_2^{\bullet-}$ ions to abstract one electron from DAB, thus initiating and propagating the oxidative reaction. Previously, Machino and Fridovich [29] reported that dihydroxyacetone phosphate oxidation by dioxygen, a reaction propagated by superoxide radical, is triggered upon addition of xanthine/xanthine oxidase as well.

That $H_2PO_4^-$ ion acts as an bifunctional acid–base catalyst of DAB enolization, as previously found for ALA [30] and AA [5], is supported by the increasing rates of oxygen uptake measured at higher concentrations of phosphate (Fig. 3B) [31]. Enolates are known to be more easily oxidized than the corresponding carbonyl forms [32]. The bell-shaped pH profile of DAB oxidation peaks at roughly 7.8, probably reflecting the overlap of two titration curves: the ascendant portion is probably due to DAB acid dissociation ($pK_a = 7.5$; inset, Fig. 3A), thus favoring enolization, and above pH 7.8, the decrease in $H_2PO_4^-$ concentration (pK_a of $H_2PO_4^- = 7.2$; Fig. 3B).

EPR spin trapping studies

EPR spin trapping studies with DMPO (Fig. 4A), POBN (Figs. 4B and C), and DBNBS (Fig. 4D) were conducted in normally aerated phosphate buffer to detect and possibly identify oxygen- and carbon-centered radical intermediates. A four-line spectrum ($\alpha_N = \alpha_H = 1.47$ mT)

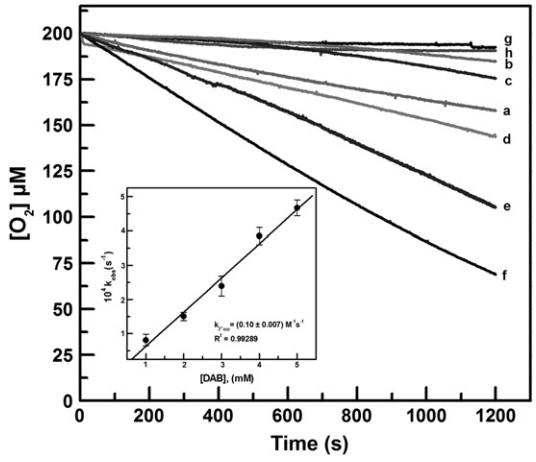

Fig. 1. Effects of metal chelator and Fe(II)EDTA or Cu(II) on oxygen consumption by DAB. Shown are the time courses of oxygen consumption by 3.0 mM DAB (curve a) alone or in presence of (curve b) 1.0 mM desferrioxamine, (curve c) 1.0 mM DTPA, (curve d) 3 μM Fe(II)EDTA, (curve e) 10 μM Fe(II)EDTA, and (curve f) 3 μM Cu(II) and the controls in the absence of DAB, (curve g) 3.0 μM Fe(II)EDTA and (curve h) 3.0 μM Cu (II). The inset shows the effect of DAB concentration on the observed autoxidation rate. Calculation of k_{obs} and $k_{2\ app}$ values assumed [O_2] of 200 μM. The data represent the mean values obtained from three independent experiments.

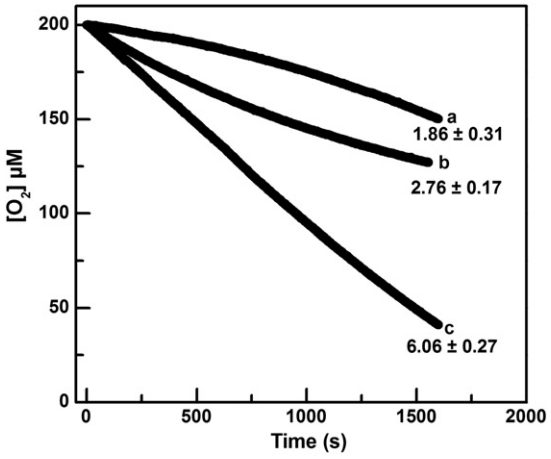

Fig. 2. Co-oxidation of DAB and xanthine in the presence of xanthine oxidase. Shown are time courses containing (curve a) 3.0 mM DAB alone, (curve b) xanthine (0.3 mM)/xanthine oxidase (25 μM), or (curve c) DAB + xanthine/xanthine oxidase. The numbers represent the mean values of reaction rates (μM min^{-1}) obtained from three independent experiments.

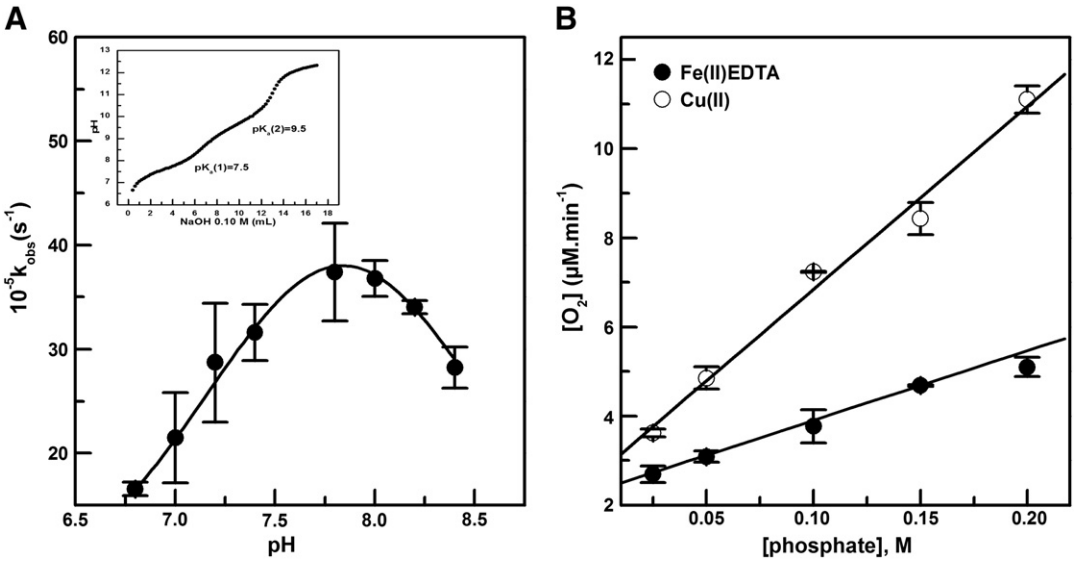

Fig. 3. pH profile of DAB oxidation and effect of phosphate. (A) Oxygen consumption by 3 mM DAB was monitored at various pH's ($n=3$). The inset shows the titration curve of DAB with NaOH in degassed Milli-Q water under a nitrogen atmosphere. (B) Oxygen consumption by 3.0 mM DAB in the presence of 3 μM Fe(II)EDTA or Cu(II), at various phosphate concentrations ($n=3$). Ionic strength was kept constant using a 0.52 M NaCl stock solution.

assignable to the DMPO–HO$^{\bullet}$ adduct [33] was found, probably formed from decomposition of the DMPO–$O_2^{\bullet-}$ adduct as suggested by the quenching effect of added 50 U ml^{-1} SOD (Fig. 4A) and methyl radical formation when in the presence of dimethyl sulfoxide (not shown). In the presence of Fe(II)EDTA or Cu(II), the spin trapping experiments revealed no significant signal intensification. However, SOD (50 U ml^{-1}) addition slightly decreased the EPR signal, and CAT (4.5 μM) completely abolished the signal from both iron- (not shown) and copper-containing (Fig. 4A) systems, which stresses the role of hydroxyl radical as a key DAB-oxidizing intermediate [7,34].

Spin trapping experiments with POBN revealed a stable major six-line signal with $\alpha_N=1.5$ mT, $\alpha_H=0.19$ mT (Fig. 4B) that can be attributed to a carbon-centered radical [33], probably the resonant enoyl radical $NH_2CH^{\bullet}COCH_2CH_2NH_3^+$, as previously showed by Monteiro et al. when studying another α-aminoketone, namely ALA [30]. A minor six-line signal with $\alpha_N=1.5$ mT, $\alpha_H=0.32$ mT also appears, which is tentatively assigned to the POBN adduct formed by trapping the oxygen-centered resonant form of the DAB enoyl radical species. Contribution of the two canonic forms of the DAB resonant enoyl radical to the EPR spectrum is simulated in Fig. 4B. Therein, the time course of the EPR spectra shows slow increase in the minor DAB adduct. Hyperfine coupling constants of POBN adducts with carbon-centered and oxygen-centered radicals are long known to exhibit similar values [33]. The concentration of the major POBN–DAB$^{\bullet}$ radical adduct increases upon increasing the DAB concentration when in presence of Fe(II)EDTA (Fig. 4C). No EPR signal was detected in the absence of metal. Additionally, the concentration effect of DAB in the Cu(II)-catalyzed reaction was not as intense as that observed with Fe(II)EDTA. Addition of SOD (50 U ml^{-1}) decreased partly the signal amplitude, whereas CAT (4.5 μM) completely abolished the EPR signal. These data support the hypothesis that both superoxide and hydroxyl radicals contribute to formation of the DAB enoyl radical.

On the other hand, DBNBS spin trapping studies endorsed the formation of a carbon-centered radical, characterized by a six-line spectrum with $\alpha_N=1.21$ mT, $\alpha_H=0.48$ mT (Fig. 4D). Accordingly, the EPR signal was intensified upon increasing the concentration of DAB and attenuated when SOD or CAT was added (data not shown). A similar EPR spectrum was obtained for a putative DBNBS–ALA$^{\bullet}$ radical adduct [36]. The observed asymmetry of the EPR spectrum depicted by Fig. 4D may be due to the presence of yet unidentified minor radicals.

Product analysis

Like ALA and AA [5,30], DAB produces NH_4^+ ion by oxidation at 3.0 mM in normally aerated 100 mM phosphate buffer, pH 7.4, at 37 °C, after 2 h incubation: 100 ± 20 μM ($n=9$) from DAB alone, 140 ± 10 μM ($n=9$) from DAB plus 3 μM Fe(II)EDTA, and 220 ± 20 μM ($n=9$) from DAB plus 3 μM Cu(II). The NH_4^+ concentration values produced in the presence of different catalysts are statistically different ($p<0.05$; ANOVA) and are expected to be limited by the concentration of dissolved oxygen, known to be approximately 200 μM in 100 mM phosphate buffer at 37 °C [26]. When studied in pure oxygen-purged buffer, the NH_4^+ concentration in the final reaction mixture of the Cu(II)-catalyzed system was threefold higher (570 ± 50 μM, $n=9$) than in air-equilibrated buffer, compared to 70 ± 10 μM ($n=9$) under argon.

The product expected from DAB oxidation, the α-oxoaldehyde oxoDAB, was not detected by HPLC analysis after derivatization with 1,2-benzenediamine [35]. Instead, as predictable by oxoDAB Schiff condensation with excess DAB, pyrrole derivatives were found by HPLC and MS analyses as shown below.

Fig. 5A shows the HPLC traces at 275 and 310 nm of DAB oxidation products after 2 h incubation in Fe(II)EDTA-containing phosphate buffer (Fig. 5A, inset). Three fractions with retention times of 4.1, 4.4, and 5.8 min were collected, corresponding to compounds with λ_{max} at 310, 275, and 310 nm, respectively. The HPLC/fluorescence detection traces allowed the product collected at 4.1 min to be identified as efficiently fluorescent compared to the others ($\lambda_{ex}=326$ nm and $\lambda_{em}=412$ nm, Fig. 5B, inset).

The fractions collected under the HPLC peaks were analyzed by mass spectrometry using direct infusion in the EPI mode (Figs. 6A, B, and C). The fraction collected at 4.1 min revealed the presence of an abundant ion with m/z 183, and a minor ion with m/z 167, whereas that collected at 5.8 min showed an m/z 187 ion as the major component, a significant concentration of the m/z 183 ion, and a minor ion with m/z 167. Finally, the fraction collected at 4.4 min ($\lambda_{max}=326$ nm) contains the molecular ion m/z 167 and a minor ion with m/z 183 (Fig. 6C). The molecular ions $[M+H]^+$ could tentatively be assigned to the condensation product of DAB with oxoDAB ($C_8H_{17}N_3O_2$, $m/z=187$), followed by its cyclization to a oxoDAB-derived pyrrolone ($C_8H_{12}N_3O_2$, $m/z=183$), whose second cyclization yields an oxoDAB dipyrrolone derivative ($C_8H_{11}N_2O_2$, $m/z=167$) (see Scheme 2, under Discussion).

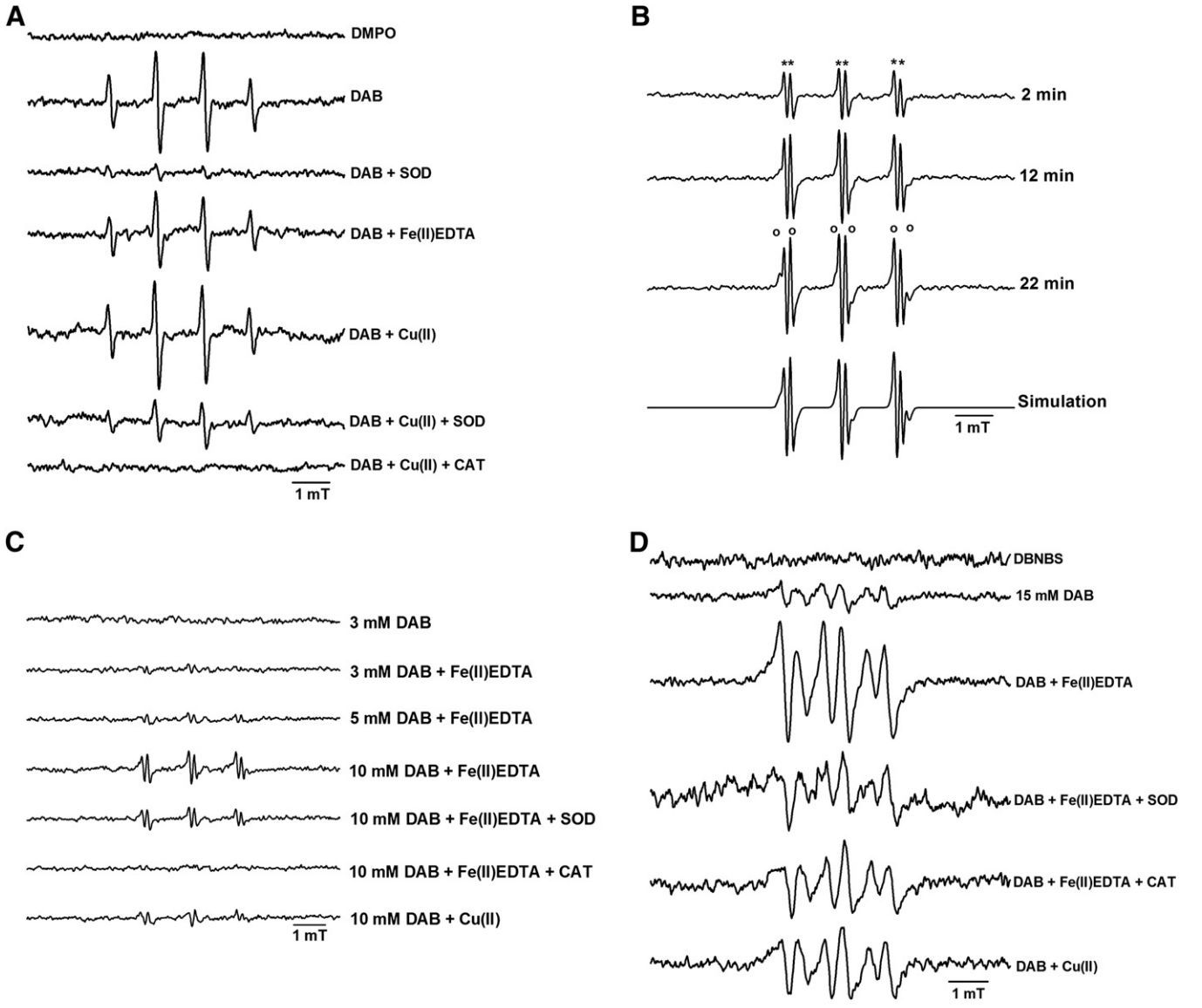

Fig. 4. EPR spin trapping studies of the metal-catalyzed aerobic oxidation of DAB. (A) EPR spectra of DMPO–radical adducts were obtained after 20-min incubation of reaction medium at 25 °C containing 3.0 mM DAB or 100 mM DMPO or DAB in the presence of 3 μM Fe(II)EDTA, 50 U ml^{-1} SOD, or 3 μM Cu(II) or Cu(II) and 50 U ml^{-1} SOD or 4.5 μM CAT. (B) Time course and spectral simulation of POBN–radical adducts formed upon incubation of 10 mM DAB in presence of 25 μM Fe(II)EDTA. *Major adduct: $\alpha_N = 1.5$ mT, $\alpha_H = 0.19$ mT. °Minor adduct: $\alpha_N = 1.5$ mT, $\alpha_H = 0.32$ mT. (C) 3.0–10 mM DAB incubated with 100 mM POBN, in presence of the 3 μM Fe(II)EDTA with and without 50 U ml^{-1} SOD or 4.5 μM CAT or in the presence of 3 μM Cu(II). (D) EPR spectra of DBNBS–radical adducts after incubation of 10 mM DAB in presence of 3 μM Fe(II)EDTA with or without 100 U SOD or 7.5 μM CAT or in the presence of Cu(II).The data represent the mean values obtained from five independent experiments.

The main fragments of each molecular ion are consistent with the assigned structures: $C_8H_{17}N_3O_2 - C_4H_9NO$, $m/z = 103$; $C_8H_{12}N_3O_2 - NH_2$, $m/z = 166$, and $C_8H_{12}N_3O_2 - COH$, $m/z = 154$; and $C_8H_{11}N_2O_2 - HO$, $m/z = 150$, and $C_8H_{11}N_2O_2 - CHO$, $m/z = 137$ (not shown). The same product profile was observed for the spent reaction mixtures obtained from DAB alone and from the Cu(II)-catalyzed DAB oxidation.

Oxidative damage to liposomes and proteins

Previous studies showed that superoxide and enoyl radicals generated by AA and ALA aerobic oxidation are able to liberate Fe (II) ion from HoSF [5,36]. Here, similar results were obtained by exposing ferritin to DAB (Fig. 7A). Iron release increased upon raising the DAB concentration and time of exposure. Accordingly, addition of 5–400 U ml^{-1} SOD to 3.0 mM DAB inhibited the initial rate of iron release by maximally 30% (Fig. 7B).

Upon treatment with DAB, quenching of tryptophan residue fluorescence from HoSF and apo-transferrin was observed (Fig. 8). A major quenching effect was observed in tryptophan residues of apo-transferrin compared with HoSF. This is probably because tryptophan residues are more exposed in apo-transferrin than in ferritin [37].

Apo-transferrin was incubated with DAB in the presence and absence of Fe(II)EDTA or Cu(II) (Figs. 8A and B). Curiously, in comparison with the Cu(II)-containing system, the apo-transferrin incubation with Fe(II) EDTA showed a higher loss of tryptophan residue fluorescence.

Fig. 9 summarizes the data obtained from the studies of DAB-induced liposome peroxidation, which was enhanced by addition of either Fe(II) EDTA or Cu(II). Relative fluorescence increased during 24-h incubation, indicating release of carboxyfluorescein into the medium. Although the experiments to evaluate lipid peroxidation by MDA determination and liposome permeabilization were carried out at different incubation times, a linear correlation between the two methods was observed ($p < 0.05$, $R^2 = 0.928$).

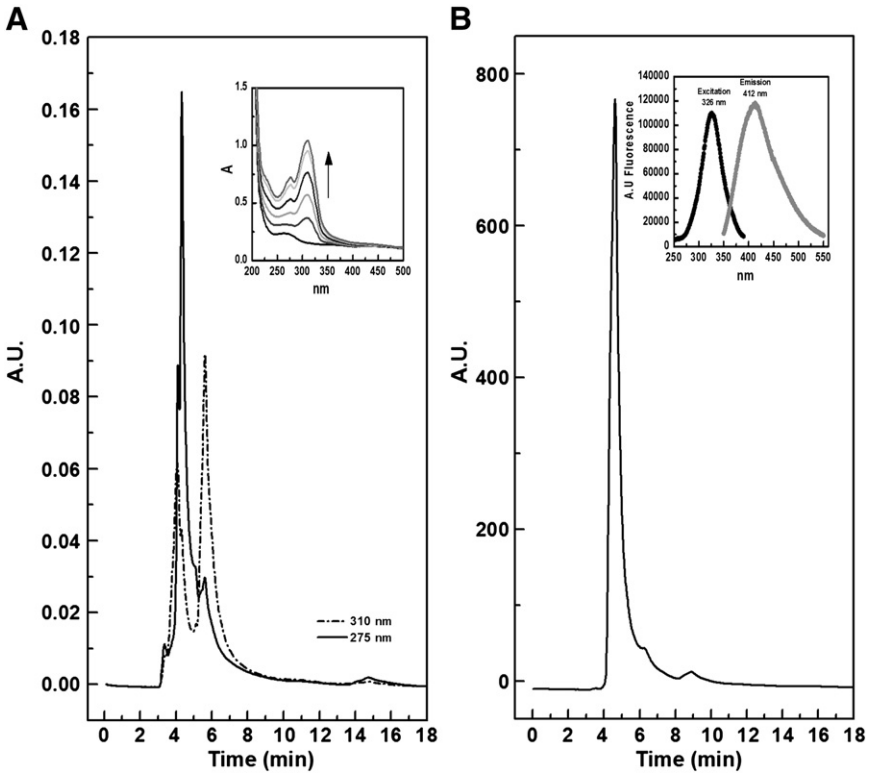

Fig. 5. HPLC separation of end-products obtained from DAB oxidation. Product analyses were performed after 2-h incubation of 3.0 mM DAB in the presence of 3 μM Fe(II)EDTA. (A) HPLC traces monitored at 275 and 310 nm. (Inset) Temporal changes in UV absorbance spectrum of DAB oxidation traced at 5-min intervals. (B) HPLC trace monitored with the fluorescence detector ($\lambda_{ex} = 326$ nm; $\lambda_{em} = 412$ nm). (Inset) Excitation and emission spectra of final reaction mixture. The data represent six independent experiments.

Cytotoxicity to culture cells

A pro-oxidant activity of DAB was examined in an in vivo system by investigating the cytotoxicity of DAB in LLC-MK2 cells, a rhesus monkey kidney epithelium cell line. The viability of these cells was dramatically affected by DAB treatment, which was evaluated as IC_{50} ca. 1.5 mM DAB upon 24 h incubation. As expected, the DAB toxicity was lower at shorter incubation times (Fig. 10A).

For comparison, the oxidative action of DAB was assessed by addition of the DAB oxidation product H_2O_2 (50–200 μM) and methylglyoxal (0.25–1.0 mM), an α-oxoaldehyde analogue of oxo-DAB, to the cell cultures. A decline in cell viability was induced by H_2O_2 and methylglyoxal in LLC-MK2 cells at concentrations in the same range as those expected from DAB oxidation products in aerated medium, in which dissolved oxygen is ca. 200 μM (Fig. 10B). These data suggest that DAB cytotoxicity to mammalian cells can be attributed to oxidative stress. Accordingly, supplementation of cell medium with CAT (4.5 μM) or aminoguanidine (25 mM), a scavenger of α-oxoaldehydes [38] and inhibitor of polyamine/diamine oxidases [39], provided significant protection of the cells against DAB toxicity (Fig. 10C). Addition of NAC, a thiol reductant, inhibited DAB-promoted loss of cell viability. There was little involvement of superoxide, however, as SOD supplementation had no effect on cell viability (Fig. 10C).

Discussion

DAB, a diamino analogue of putrescine, is a competitive inhibitor of ODC in several pathogenic microorganisms such as *T. cruzi*[11], *L. amazonensis*[12], *G. lamblia*[13], *Entamoeba invadens*[40], *Aspergillus nidulans*[15], and *Candida albicans*[41]. Therefore, administration of millimolar DAB to several types of cells is expected to cause a significant decrease in polyamine contents, consequently leading to a notable decline in cell proliferation [11–13]. Accordingly, DAB reportedly promotes cell architecture disorganization, mitochondrial dysfunction, and increased lipid peroxidation [11,13]. In this context, it is important to clarify the relationship of DAB cytotoxicity and oxidative stress.

We demonstrate here that DAB undergoes metal-catalyzed oxidation propagated by $O_2^{\bullet-}$ yielding oxyradicals (Figs. 1–4), NH_4^+ ion, and oxoDAB, a potentially cytotoxic α-oxoaldehyde [42] (Scheme 2). This reaction is preceded by phosphate-catalyzed DAB enolization (Fig. 3A). In vivo, one can predict an electrophilic attack of oxoDAB on proteins and DNA [10] followed by covalent modification ultimately leading to loss of protein function and DNA mutation, respectively. This hypothesis is supported here by Schiff conjugation of oxoDAB with DAB itself to pyrrolone derivatives, as demonstrated by HPLC–MS studies (Figs. 5 and 6).

The rates of oxygen consumption by DAB in the presence of transition metal ions (Figs. 1 and 3B) indicate that the reaction in the presence of Cu(II) is at least three times faster than with the same concentration of Fe(II)EDTA. The observed higher inhibition by added SOD or semicarbazide, both efficient superoxide radical scavengers, in the Fe(II)EDTA-catalyzed DAB than with Cu(II) is consistent with a superoxide-propagated process (Table 1). Similar effects of SOD and CAT in the iron-catalyzed oxidation of AA and ALA have been observed previously as well [5,30]. In turn, the observed inhibitory effects of CAT and GSH on metal-catalyzed DAB oxidation indicate that H_2O_2 plays a more important role in the Cu(II)-catalyzed reaction than in that with Fe(II)EDTA, perhaps because of higher superoxide dismutation catalyzed by Cu(II) [43] (Scheme 2). Probably, oxidation of enol DAB in presence of Fe(II)EDTA or Cu(II) occurs by two contributing mechanisms. Two-electron transfer from a DAB–Cu(I) complex to dioxygen producing H_2O_2 prevails with copper, whereas the DAB–Fe(II) complex would transfer just one electron to dioxygen to form superoxide radical, one of the propagation intermediates and a source of H_2O_2 by dismutation. In both cases, DAB enoyl radical is formed and

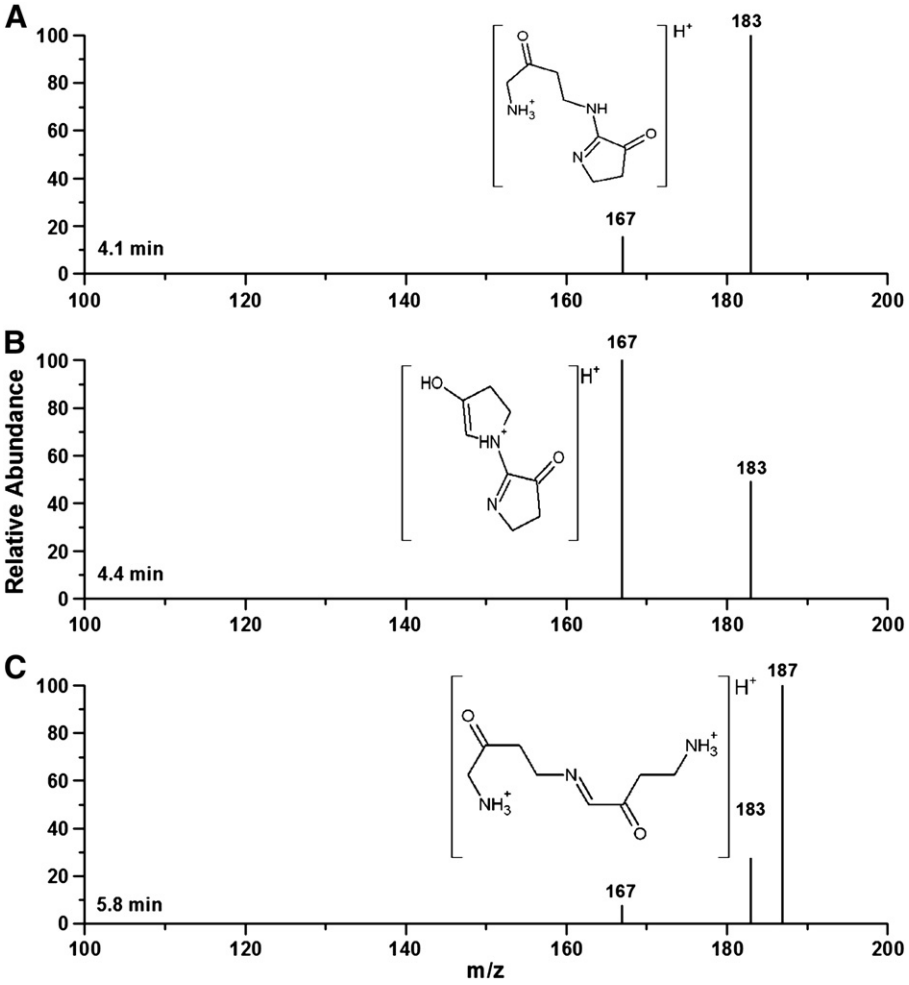

Fig. 6. MS analysis of the HPLC fractions of DAB oxidation end-products. (A) Fraction 4.1 min, corresponding to the 310 nm absorption peak and fluorescence (326/412 nm). (B) Fraction 4.4 min peak elution, corresponding to the 275 nm peak. (C) Fraction 5.8 min is related to the 310 nm peak. The data represent six independent experiments.

consumed by dioxygen, thus propagating the reaction. Accordingly, SOD inhibits iron-catalyzed oxygen consumption but exhibits little effect on the presence of copper.

The EPR spin trapping experiments with DMPO (Fig. 4A) confirm the hypothesis of superoxide and hydroxyl radical production by DAB oxidation. The slight effect of SOD and remarkable inhibition by CAT on the amplitude of the four-line EPR signal characteristic of a DMPO–$HO^{\bullet}$ adduct support the idea of H_2O_2 as a key agent in the metal-catalyzed DAB oxidation. Moreover, experiments with POBN and DBNBS suggest that the formation of the hypothetical resonant enoyl radical ($DAB^{\bullet}$) is indeed dependent on ROS, in accordance with the observed quenching effect of SOD or CAT on the EPR signal intensities (Scheme 2, Figs. 4B, C, and D). These results partly reproduce earlier studies under similar experimental conditions with ALA and AA, two other α-aminoketones [5,30,36].

We also show here that DAB induces oxidative damage to liposomes and iron-carrier proteins, namely ferritin and transferrin. Acquiring iron is a fundamental step in the development of a pathogen [44]. All iron that protozoan parasites need for growth is delivered by transferrin or ferritin of the host cells [45]. Ferritin is an iron-storage protein that functions in iron homeostasis and detoxification by sequestering iron within its core [46,47]. We suggest that DAB enoyl radical is the main agent of Fe(II) release from ferritin because increasing amounts of SOD added to the reaction mixture reached a plateau at 30% inhibition (Fig. 7B). This was also verified when conducting similar experiments with AA and ALA [5,36]. Furthermore, α-aminoketones reportedly promote structural damage to the ferritin structure, leading to loss of α-helix content and concomitant decrease in ferroxidase activity and tryptophan fluorescence intensity [48,49]. DAB-induced decay of tryptophan fluorescence of apo-transferrin, a crucial protein synthesized to bind excess iron in the blood circulation, was also observed (Figs. 8B and C) [50]. The observed higher quenching of tryptophan fluorescence in apo-transferrin than in ferritin may result from the facts that (i) apo-transferrin (80 kDa) is much smaller than ferritin (460 kDa), implying that its tryptophan residues are more exposed to the medium, and (ii) the absence of iron in apo-transferrin contributes positively to the quantum yield of fluorescence of its tryptophan residues [37,51].

Possible pro-oxidant activity of DAB was tested on the viability of LLC-MK2 mammalian cells exposed to the toxicant. A mammalian cell line was chosen as a first step to further investigate the microbicide action of DAB on the same cell line infected with *T. cruzi* DAB showed to be cytotoxic to the cell cultures with an IC_{50} value of 1.5 mM during 24 h incubation (Fig. 10A). That the DAB oxidation products are implicated in the observed cytotoxicity was demonstrated by the protective effect of added CAT and aminoguanidine (Fig. 10C). Considering that the DAB oxidation rate constant measured in vitro is low ($k_{2\,app} = 0.10\ M^{-1}\,s^{-1}$), it is possible that internalized DAB is preferentially oxidized by polyamine/diamine oxidases present in the cell [13,52]. Accordingly, polyamine/diamine oxidases catalyze the oxidative deamination of biogenic amines and polyamines generating stoichiometric amounts of H_2O_2, NH_4^+ and a correspondent aldehyde, which are able to induce cell

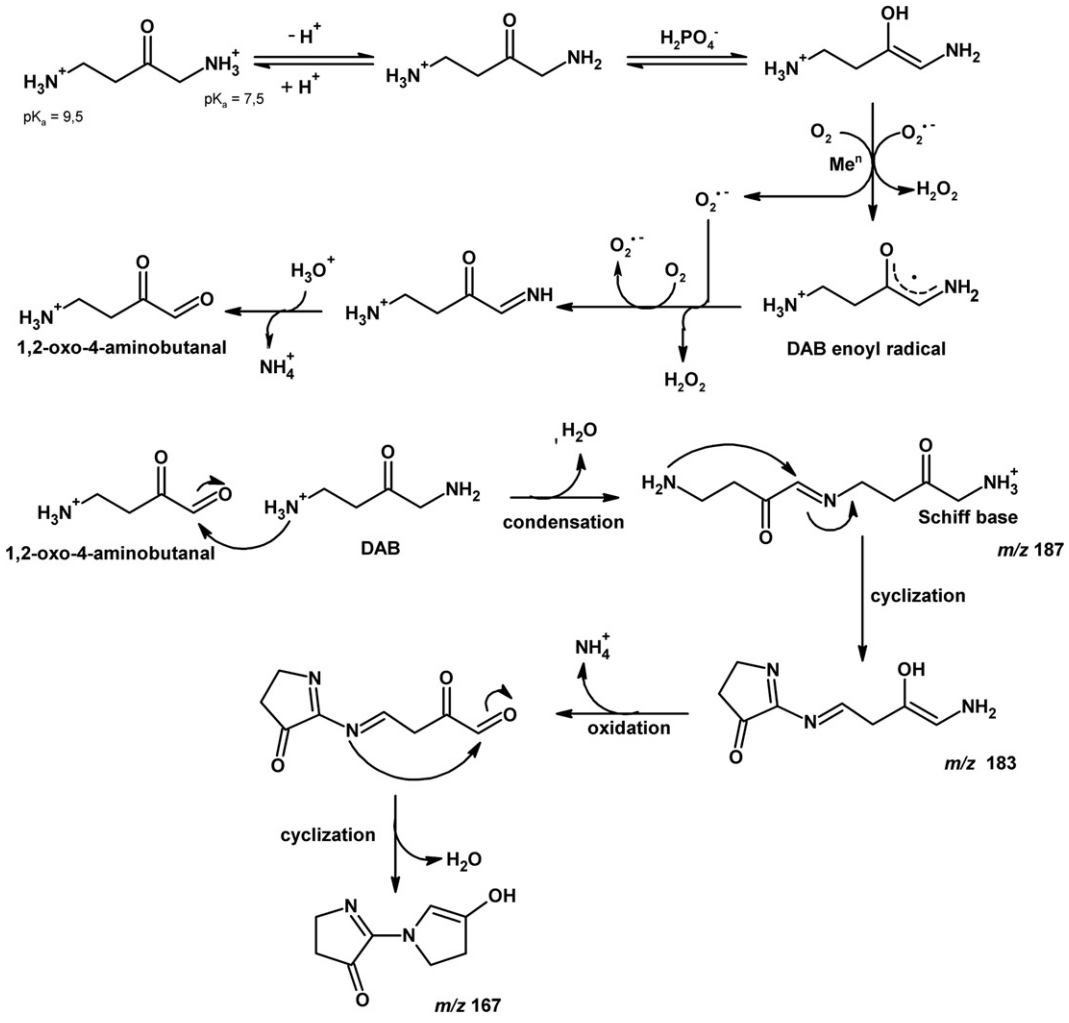

Scheme 2. Chemical mechanism proposed for metal-catalyzed DAB aerobic oxidation.

death in several cell lines [53]. The putative pro-oxidant effects of DAB reported here rely on the fact that ODC is a tightly regulated and short-lived enzyme (lifetime in the range 10–20 min) in mammalian cells [54], which thereby may minimize the effect of DAB as an ODC inhibitor.

Menezes et al. [11] and Maia et al. [13] reported that DAB administration to *T. cruzi* epimastigotes and to *G. lamblia* cultures inhibits cell proliferation, increases the extent of lipid peroxidation, induces remarkable mitochondrial destruction, and promotes cell architecture

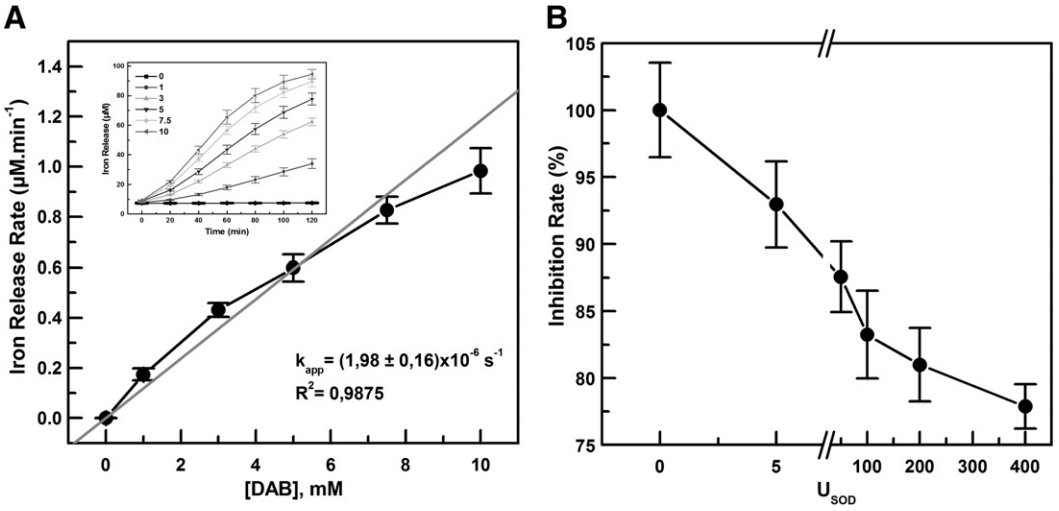

Fig. 7. DAB effect on iron release from ferritin. HoSF (2.5 mg ml^{-1}) was incubated with DAB (0–10 mM) for 2 h. (A) Dependence of iron release rate on DAB concentration. (B) Effect of SOD (5–400 U ml^{-1}) on the rate of iron release in the presence of 3.0 mM DAB. The data represent the mean values obtained from three independent experiments.

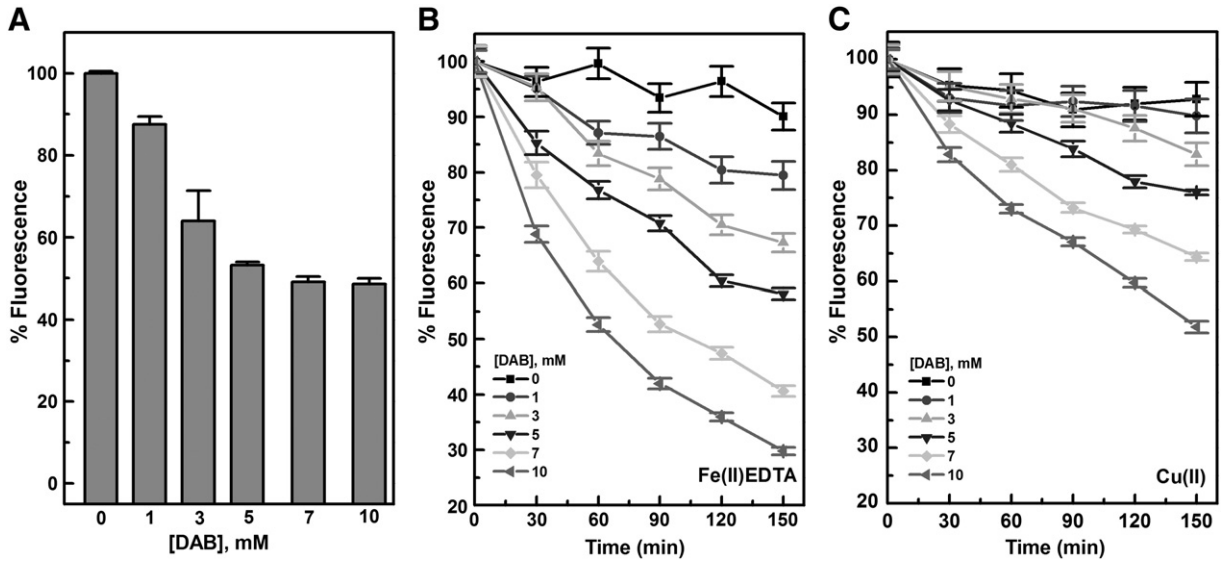

Fig. 8. DAB effect on the intensity of tryptophan fluorescence. (A) HoSF (2.5 mg ml^{-1}) and (B and C) apo-transferrin were incubated for 120 min with 1.0–10 mM DAB. Apo-transferrin was incubated in the presence of 3 μM Fe(II)EDTA (B) or Cu(II) (C). The data represent the mean values obtained from three independent experiments.

disorganization. Further studies are demanded to clarify the mechanism and organelle targets of DAB toxicity and pro-oxidative effects on *T. cruzi* cells. Here we show that DAB indeed causes peroxidation and permeabilization of biomimetic vesicles and covalent modifications of ferritin and apo-transferrin. Chemical damage to other proteins, DNA, and membranes by DAB as well as alterations in iron and copper homeostasis probably related to mitochondrial permeabilization can be anticipated for DAB from previous studies carried out with ALA and AA [6 and references therein]. In conclusion, we hypothesize that DAB is toxic to a different sort of cells, including mammalian cells, not only by interfering in their polyamine biosynthesis but also by altering their redox balance.

Acknowledgments

This work was supported by the Fundação de Amparo à Pesquisa do Estado de São Paulo, the Conselho Nacional de Desenvolvimento Científico e Tecnológico, the Coordenação de Aperfeiçoamento de Pessoal de Nível Superior, and the INCT Processos Redox em Biomedicina–Redoxoma. We are grateful to Dr. Brian Bandy (University of Saskatchewan, Saskatoon, SA. Canada) and Dr. Avishek Adhikari (Stanford University, Stanford, CA, USA) for kindly reading the manuscript and to Rita Tokikawa and Julio Massari Filho for helpful discussions and to Sandra M. Vaz for kindly providing DBNBS.

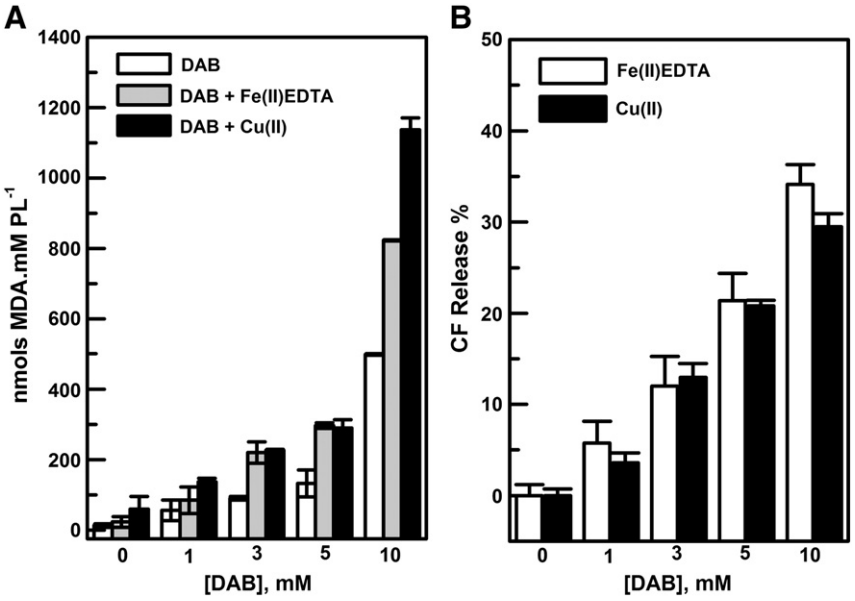

Fig. 9. Lipid peroxidation induced by DAB at various concentrations. Liposomes made from phosphatidylcholine:cardiolipin (80:20) were incubated in 100 mM phosphate buffer, pH 7.4, at 37 °C, in the presence of various DAB concentrations. (A) Lipid peroxidation evaluated as TBA-reactive substances after 60 min incubation. (B) Liposome permeabilization evaluated by the percentage of carboxyfluorescein released after 24 h incubation. The data represent the mean values obtained from three independent experiments.

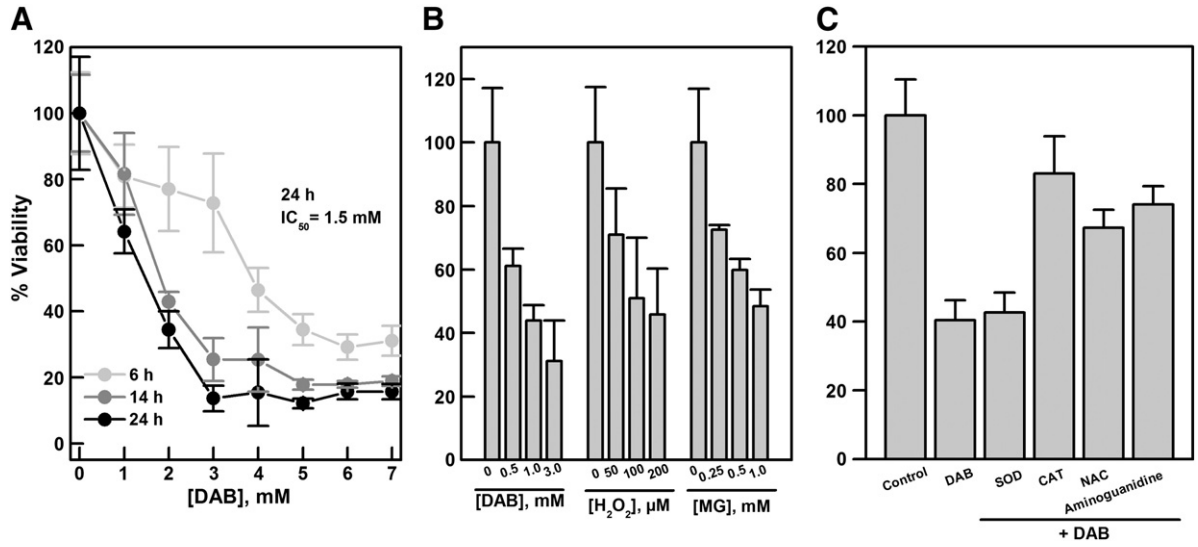

Fig. 10. DAB cytotoxicity to LLC-MK2 cells. (A) Viability curve at various concentrations of DAB and times of exposure. (B) Comparison of DAB, H_2O_2, and methylglyoxal (MG) toxicities. (C) Effect of ROS scavengers on DAB-induced cytotoxicity. Epithelial cells, lineage LLC-MK2, were seeded at a density 5×10^4 cells per well, in 24-well plates, 24 h before treatments. All DAB (3.0 mM) assays were carried out in MEM, supplemented with 2% FBS at 37 °C and 5% CO_2. SOD, 50 U ml^{-1}; CAT, 4.5 µM; NAC, 5 mM; and aminoguanidine, 25 mM. Cell viability was assessed by MTT reduction levels in comparison with control. The data represent the mean values obtained from three independent experiments ($n = 6$).

References

[1] Sassa, S. Modern diagnosis and management of the porphyrias. *Br. J. Haematol.* **135:**281–292; 2006.
[2] Hindmarsh, J. T. The porphyrias: recent advances. *Clin. Chem.* **32:**1255–1263; 1986.
[3] Kalapos, M. P. The tanden of free radicals and methylglyoxal. *Chem. Biol. Interact.* **171:**251–271; 2008.
[4] Yu, P. H.; Wang, M.; Fan, H.; Deng, Y.; Gubisne-Haberle, D. Involvement of SSAO-mediated deamination in adipose glucose transport and weight gain in obese diabetic KKAy mice. *Am. J. Physiol. Endocrinol. Metab.* **286:**E634–E641; 2004.
[5] Dutra, F.; Knudsen, F. S.; Curi, D.; Bechara, E. J. H. Aerobic oxidation of aminoacetone, a threonine catabolite: iron catalysis and coupled iron release from ferritin. *Chem. Res. Toxicol.* **14:**1323–1329; 2001.
[6] Bechara, E. J.; Dutra, F.; Cardoso, V. E.; Sartori, A.; Olympio, K. P.; Penatti, C. A.; Adhikari, A.; Assunção, N. A. The dual face of endogenous alpha-aminoketones: pro-oxidizing metabolic weapons. *Comp. Biochem. Physiol. C Toxicol. Pharmacol.* **146:**88–110; 2007.
[7] Douki, T.; Onuki, J.; Medeiros, M. H.; Bechara, E. J. H.; Cadet, J.; Di Mascio, P. Hydroxyl radicals are involved in the oxidation of isolated and cellular DNA bases by 5-aminolevulinic acid. *FEBS Lett.* **428:**93–96; 1998.
[8] Douki, T.; Onuki, J.; Medeiros, M. H.; Bechara, E. J.; Cadet, J.; Di Mascio, P. DNA alkylation by 4,5-dioxovaleric acid, the final oxidation product of 5-aminolevulinic acid. *Chem. Res. Toxicol.* **11:**150–157; 1998.
[9] Uchida, K. Role of reactive aldehyde in cardiovascular diseases. *Free Radic. Biol. Med.* **28:**1685–1696; 2000.
[10] Thornalley, P. J. Dicarbonyl intermediates in the Maillard reaction. *Ann. N.Y. Acad. Sci.* **1043:**111–117; 2005.
[11] Menezes, D.; Valentim, C.; Oliveira, M. F.; Vannier-Santos, M. A. Putrescine analogue cytotoxicity against *Trypanosoma cruzi*. *Parasitol. Res.* **98:**99–105; 2006.
[12] Vannier-Santos, M. A.; Menezes, D.; Oliveira, M. F.; Mello, F. G. The putrescine analogue 1,4-diamino-2-butanone affects polyamine synthesis, transport, ultrastructure and intracellular survival in *Leishmania amazonensis*. *Microbiology* **154:**3104–3111; 2008.
[13] Maia, C.; Lanfredi-Rangel, A.; Santana-Anjos, K. G.; Oliveira, M. F.; Souza, W.; Vannier-Santos, M. A. Effects of a putrescine analog on *Giardia lamblia*. *Parasitol. Res.* **103:**363–370; 2008.
[14] Reis, I. A.; Martinez, M. P.; Yarlett, N.; Johnson, P. J.; Silva-Filho, F. C.; Vannier-Santos, M. A. Inhibition of polyamine synthesis arrests trichomonad growth and induces destruction of hydrogenosomes. *Antimicrob. Agents Chemother.* **43:** 1919–1923; 1999.
[15] Stevens, L.; McKinnon, I. M.; Winther, M. The effects of 1,4-diaminobutanone on polyamine synthesis in *Aspergillus nidulans*. *FEBS Lett.* **75:**180–182; 1977.
[16] Bhattacharya, S.; Ray, R. M.; Johnson, L. R. Role of polyamines in p53-dependent apoptosis of intestinal epithelial cells. *Cell Signaling* **21:**509–522; 2009.
[17] Bouchereau, A.; Aziz, A.; Larher, F.; Martin-Tanguy, J. Polyamines and environmental challenges: recent development. *Plant Sci.* **140:**103–125; 1999.
[18] Kusano, T.; Berberich, T.; Tateda, C.; Takahashi, Y. Polyamines: essential factors for growth and survival. *Planta* **228:**367–381; 2008.
[19] Augusto, O.; Bonini, M. G.; Amanso, A. M.; Linares, E.; Santos, C. C.; Menezes, S. L. Nitrogen dioxide and carbonate radical anion: two emerging radicals in biology. *Free Radic. Biol. Med.* **32:**841–859; 2002.
[20] Itakura, K.; Osaka, T.; Uchida, K. Structure of a fluorescent compound formed from 4-hydroxy-2-nonenal and N-hippuryllysine: a model for fluorophores derived from protein modifications by lipid peroxidation. *J. Org. Chem.* **63:**185–187; 2008.
[21] Oteiza, P. I.; Kleinman, C. G.; Demasi, M.; Bechara, E. J. H. 5-Aminolevulinic acid induces iron release from ferritin. *Arch. Biochem. Biophys.* **316:**607–611; 1995.
[22] Bradford, M. M. A rapid and sensitive method for the quantitation of microgram quantities of protein utilizing the principle of protein–dye binding. *Anal. Biochem.* **72:**248–254; 1979.
[23] Oteiza, P. I.; Bechara, E. J. H. 5-Aminolevulinic acid induces lipid peroxidation in cardiolipin-rich liposomes. *Arch. Biochem. Biophys.* **305:**282–287; 1993.
[24] Fukunaga, K.; Yoshida, M.; Nakazono, N. A simple, rapid, highly sensitive and reproducible quantification method for plasma malondialdehyde by high-performance liquid chromatography. *Biomed. Chromatogr.* **12:**300–303; 1998.
[25] Puntel, R. L.; Roos, D. H.; Grotto, D.; Garcia, S. C.; Nogueira, C. W.; Rocha, J. B. T. Antioxidant properties of Krebs cycle intermediates against malonate pro-oxidant activity in vitro: a comparative study using the colorimetric method and HPLC analysis to determine malondialdehyde in rat brain homogenates. *Life Sci.* **81:** 51–62; 2007.
[26] Robinson, J.; Cooper, J. M. Method of determining oxygen concentrations in biological media, suitable for calibration of the oxygen electrode. *Anal. Biochem.* **33:**390–399; 1970.
[27] Miller, D. M.; Buettner, G. R.; Aust, S. D. Transition metals as catalysts of autoxidation reactions. *Free Radic. Biol. Med.* **8:**95–108; 1990.
[28] Qian, S. Y.; Buettner, G. R. Iron and dioxygen chemistry is an important route to initiation of biological free radical oxidations: an electron paramagnetic resonance spin trapping study. *Free Radic. Biol. Med.* **26:**1447–1456; 1999.
[29] Mashino, T.; Fridovich, I. Superoxide radical initiates the autoxidation of dihydroxyacetone. *Arch. Biochem. Biophys.* **254:**547–551; 1987.
[30] Monteiro, H. P.; Abdalla, D. S. P.; Augusto, O.; Bechara, E. J. H. Free radical generation during 5-aminolevulinic acid autoxidation: induction by hemoglobin and connections with porphyrinpathies. *Arch. Biochem. Biophys.* **271:**206–216; 1989.
[31] Bruice, P. Y. Role of acidity of the ketone, carbinolamine, or imine: catalysis of enolization of 2,4-pentanedione and 3-methyl-2,4-pentanedione by oxyanions and by primary, secondary and tertiary amines. *J. Am. Chem. Soc.* **112:**7361–7368; 1990.
[32] Bechara, E. J. H.; Oliveira, O. M. M. F.; Duran, N.; Baptista, R. C.; Cilento, G. Peroxidase catalyzed generation of triplet acetone. *Photochem. Photobiol.* **30:** 101–110; 1979.
[33] Buettner, G. R. Spin trapping: ESR parameters of spin adducts. *Free Radic. Biol. Med.* **3:**259–303; 1987.
[34] Su, M.; Yang, Y.; Yang, G. Quantitative measurement of hydroxyl radical induced DNA double-strand breaks and the effect of *N*-acetyl-L-cysteine. *FEBS Lett.* **580:** 4136–4142; 2006.
[35] Okado-Matsumoto, A.; Fridovich, I. The role of alpha, beta-dicarbonyl compounds in the toxicity of short chain sugar. *J. Biol. Chem.* **275:**34853–34857; 2000.
[36] Rocha, M. E. M.; Ferreira, A. M. D. C.; Bechara, E. J. H. Roles of phosphate and an enoyl radical in ferritin iron mobilization by 5-aminolevulinic acid. *Free Radic. Biol. Med.* **29:**1272–1279; 2000.
[37] He, Q. Y.; Mason, A. B.; Lyons, B. A.; Tam, B. M.; Nguyen, V.; MacGillivray, R. T.; Woodworth, R. C. Spectral and metal-binding properties of three single-point tryptophan mutants of the human transferrin N-lobe. *Biochem. J.* **354:**423–429; 2001.
[38] Thornalley, P. J. Use of aminoguanidine (Pimagedine) to prevent the formation of advanced glycation end products. *Arch. Biochem. Biophys.* **419:**31–40; 2003.

[39] Brunton, V. G.; Grant, M. H.; Wallace, H. M. Mechanisms of spermine toxicity in baby-hamster kidney (BHK) cells: the role of amine oxidases and oxidative stress. *Biochem. J.* **280:**193–198; 1991.
[40] Calvo-Méndez, C.; Villagómez-Castro, J. C.; López-Romero, E. Ornithine decarboxylase activity in *Entamoeba invadens*. *Int. J. Parasitol.* **23:**847–852; 1993.
[41] Ueno, Y.; Fukumatsu, M.; Ogasawara, A.; Watanabe, T.; Mikakami, T.; Matsumoto, T. Hyphae formation of *Candida albicans* is regulated by polyamines. *Biol. Pharm. Bull.* **27:**890–892; 2004.
[42] Abordo, E. A.; Minhas, H. S.; Thornalley, P. J. Accumulation of α-oxoaldehydes during oxidative stress: a role in cytotoxicity. *Biochem. Pharmacol.* **58:**641–648; 1999.
[43] Halliwell, B.; Gutteridge, J. M. C. Free Radicals in Biology and Medicine, 4th edition. Oxford Univ. Press, New York; 2007.
[44] Doherty, C. P. Host–pathogen interactions: the role of iron. *J. Nutr.* **137:** 1341–1344; 2007.
[45] Wilson, M. E.; Britigan, B. E. Iron acquisition by parasitic protozoa. *Parasitol. Today* **14:**93–95; 1998.
[46] Crichton, R. R.; Declercq, J. P. X-ray structures of ferritins and related proteins. *Biochim. Biophys. Acta* **1800:**706–718; 2010.
[47] Harrison, P. M.; Arosio, P. M. The ferritins: molecular properties, iron storage function and cellular regulation. *Biochim. Biophys. Acta* **1275:**161–203; 1996.
[48] Dutra, F.; Araki, D.; Bechara, E. J. H. Aminoacetone induces loss of ferritin ferroxidase and iron uptake activities. *Free Radic. Res.* **37:**1113–1121; 2003.
[49] Rocha, M. E. M.; Dutra, F.; Bandy, B.; Baldini, R. L.; Gomes, S. L.; Faljoni-Alario, A.; Líria, C. W.; Miranda, M. T. M.; Bechara, E. J. H. Oxidative damage to ferritin by 5-aminolevulinic acid. *Arch. Biochem. Biophys.* **409:**349–356; 2003.
[50] Kohgo, Y.; Ikuta, K.; Ontake, T.; Torimoto, Y.; Kato, J. Body iron metabolism and pathophysiology of iron overload. *Int. J. Hematol.* **88:**7–15; 2008.
[51] Stefanini, S.; Chiancone, E.; Arosio, P.; Finazzi-Agro, A.; Antonini, E. Structural heterogeneity and subunit composition of horse ferritins. *Biochemistry* **21:** 2293–2299; 1982.
[52] Agostinelli, E.; Arancia, G.; Vedova, L. D.; Belli, F.; Marra, M.; Salvi, M.; Toninello, A. The biological functions of polyamine oxidation products by amine oxidases: perspectives of clinical applications. *Amino Acids* **27:**347–358; 2004.
[53] Seiler, N. Catabolism of polyamines. *Amino Acids* **26:**217–233; 2004.
[54] Manen, C. A.; Russell, D. H. Regulation of RNA polymerase I activity by ornithine decarboxylase. *Biochem. Pharmacol.* **26:**2379–2384; 1977.